Geomechanics and Engineering, *Vol. 29, No. 1 (2022) 25-40*
https://doi.org/10.12989/gae.2022.29.1.025

Responses of high-rise building resting on piled raft to adjacent tunnel at different depths relative to piles

Mukhtiar Ali Soomro*[1], Naeem Mangi[2], Aftab Hameed Memon[2] and Dildar Ali Mangnejo[2]

[1]*School of Mechanics and Civil Engineering, China University of Mining and Technology, Xuzhou, Jiangsu, P. R. China*
[2]*Department of Civil Engineering, Quaid-e-Awam University of Engineering, Science & Technology, Sindh, Pakistan*

(Received October 26, 2021, Revised February 9, 2022, Accepted February 15, 2022)

Abstract. In this study, 3D coupled-consolidation numerical parametric study was conducted to predict the deformation mechanism of a 20 storey building sitting on (4×4) piled raft (with length of piles, L_p=30 m) to adjacent 6 m diameter (D) tunnelling in stiff clay. The influences of different tunnel locations relative to piles (i.e., z_t/L_p) were investigated in this parametric study. In first case, the tunnel was excavated near the pile shafts with depth of tunnel axis (z_t) of 9 m (i.e., z_t/L_p). In second and third cases, tunnels were driven at z_t of 30 m and 42 m (i.e., z_t/L_p = 1.0 and 1.4), respectively. An advanced hypoplastic clay model (which is capable of taking small-strain stiffness in account) was adopted to capture soil behaviour. The computed results revealed that tunnelling activity adjacent to a building resting on piled raft caused significant settlement, differential settlement, lateral deflection, angular distortion in the building. In addition, substantial bending moment, shear forces and changes in axial load distribution along pile length were induced. The findings from the parametric study revealed that the building and pile responses significantly influenced by tunnel location relative to pile.

Keywords: 3D parametric study; 20 storey building: piled raft; different tunnel depths relative to pile length; tunnelling

1. Introduction

It is not unusual situation for a tunnelling activity in metropolitan cities to be performed very close to a high-rise building which could be founded on deep foundation such as piles and piled raft. It is highly likely that tunnelling-induced ground movement and stress relief may lead to severe damage and might result in collapse of structure. Therefore, it is necessary for geotechnical engineers to assess the detrimental effects of tunnelling activity on nearby building. The tunnelling induced ground movement and its effects on the building resting on piled raft is a complex soil-structure interaction problem (Bai *et al*. 2021b). Several researchers have studied this complex problem by means of different approaches. Current design approaches for the assessment of damages (i.e., induced deflection and tensile strain) on building due to tunnelling are based on semi-empirical (Franza *et al*. 2017, Franza and DeJong 2019). This approach is based on assumption that the deformation pattern of structure will follow the induced green-field settlement trough due to tunnelling (Boscardin and Cording 1989, Burland *et al*. 1977, O'Reilly and New 1982, Peck 1969). In another approach, researchers assumed the building as an elastic Timoshenko beam (Burd *et al.* 2000, Franzius *et al*. 2004, 2006, Pickhaver *et al.* 2010, Potts and Addenbrooke 1997, Bai *et al.* 2021c). However, this method is only applicable to load bearing structures. The limitations and applicability of the approach to framed building exists. In addition, experimental studies were carried to understand responses of building to adjacent tunnelling (Caporaletti *et al*. 2005, Farrell 2010, Franza and Marshall 2018, Ritter *et al*. 2020, Taylor and Grant 1998, Taylor *et al*. 2001, Lee *et al*. 2016, Heama *et al.* 2021). Recently, the evaluation of tunnelling effects on building has been studied by means of numerical (Boldini *et al*. 2018, Fu *et al*. 2014, 2018, Giardina *et al.* 2013, Goh and Mair 2011, Son and Cording 2007, Yiu *et al*. 2017, Soomro 2021a, Soomro *et al*. 2021b, Soomro *et al,* 2021c, Soomro *et al.* 2020). These studies showed that when tunnelling is performed close to a pre-existing pile, pile behaviour is more affected than when the tunnel is located in the transverse direction of the piles. In addition, axial pile forces with depth are reduced, with tunnel advancement indicating tunnelling-induced tensile force on piles. Among those numerical studies, however, responses of framed building to tunnelling were reported in a limited number of studies. Most of these aforementioned research studies only examined the tunnelling effects on building founded on shallow footings (Boldini *et al.* 2018, Fu *et al.* 2014). Therefore, there is a gap of systematic research on the responses of a high-rise building subjected to live load and resting on piled raft to advancement of adjacent tunnelling. The paper aims to understand the responses of a 20 storey building to ground movement due to tunnelling- induced stress relief. To achieve this, three-dimensional coupled-consolidation finite element analysis was conducted. The building deformation (i.e., differential settlement, deflection and crack damage) and piled raft (i.e., induced bending moment and shear forces in the piles and induced shear and

*Corresponding author, Professor
E-mail: eng.soomro@gmail.com

http://www.techno-press.org/?journal=gae&subpage=7
ISSN: 2005-307X (Print), 2092-6219 (Online)

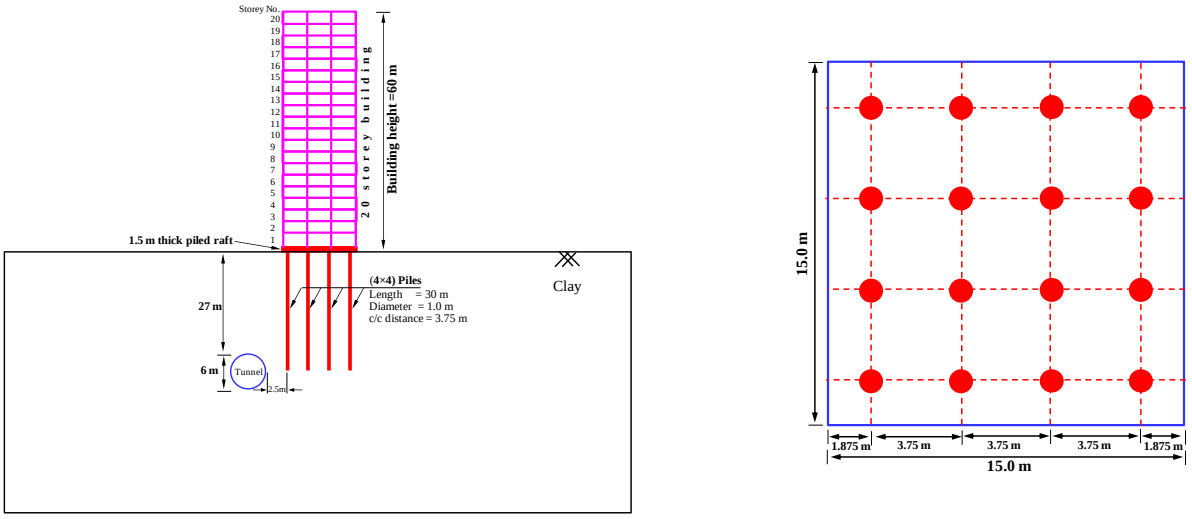

(a) (b)

Fig. 1 (a) General setup of building, piled raft and tunnel for a typical case T (b) Piles arrangement in raft

Table 1 Summary of numerical simulations

Simulation ID	z_t/L_p	C/D	Remarks
S	0.3	1.0	The tunnel was excavated near the pile shaft.
T	1.0	4.5	The tunnel was excavated next to the pile toe
B	1.4	6.5	The tunnel was excavated below the pile toe

Note: z_t= depths of tunnel axis; L_p= pile length; C/D= cover to diameter of tunnel ratio

Table 2 Summary of numerical simulations (Rasouli and Fatahi 2019)

Section type	Column I	Column II	Column III	Column IV	Column V	Column VI	Slab
Dimension (m)	0.75×0.75	0.70×0.70	0.65×0.65	0.6×0.6	0.55×0.55	0.50×0.50	13.5×13.5×0.25
Distribution level	1-3	4-7	8-11	12-15	16-18	19-20	All levels
Cross-sectional area, A (m^2)	0.5625	0.49	0.4225	0.36	0.3025	0.25	0.25 (1 m width)
Flexural rigidity, EI ($GPa.m^4$)	0.794	0.602	0.448	0.325	0.230	0.157	0.039

normal tractions) were presented and discussed.

2. Development of three-dimensional finite element model

2.1 General

In this study, three-dimensional numerical parametric modelling technique was used to construction of tunnels (with different cover-to-diameter C/D ratios) adjacent to a 20 storey high rising building which is resting on a (4×4) piled raft foundation in stiff clay. 3D coupled-consolidation analyses were adopted in this parametric study which is consists of three different cases. In first case, a 6 m diameter tunnel was excavated near the pile shaft with cover depth of 6 m (i.e., C/D= 1.0). For simplicity, this case is referred as case S hereinafter. In second and third cases (which are named as cases T and B), tunnels were driven at cover depths of 27 m and 39 m (i.e., C/D= 4.5 and 6.5), respectively. Table 1 summarized all three cases conducted in this parametric study. Abaqus software package version 6.14-2 was used to conduct finite element analyses in this study. Fig. 1(a) illustrates the general setup of the 20 storey building founded on piled raft and an adjacent tunnel in a typical case T. A 60-m high, 12-m wide 20-storey, concrete building with three spans in each direction was selected for this parametric study. The building was founded on a square raft; 15 m wide and 1.5 m thick supported by a group of piles in a 4×4 configuration with centre-to-centre distance of 3.75 m (see Fig. 1(b)). The diameter (d_p) and length (L_p) of each pile were 1 m and 30 m, respectively. The clear distance between tunnel and the closest pile to the tunnel was 2.5 m ($2.5d_p$). Since the prime objective of this parametric study is to assess the impact of tunnelling on the 20 storey building under dead and live loads. The live load of 5 kPa [AS1170.1] was adopted in this study. With this adopted piled raft system, the numerical prediction showed that settlement of the building due to dead and live load was 45.2 mm ($4.52\%d_p$) which is within the limit of the

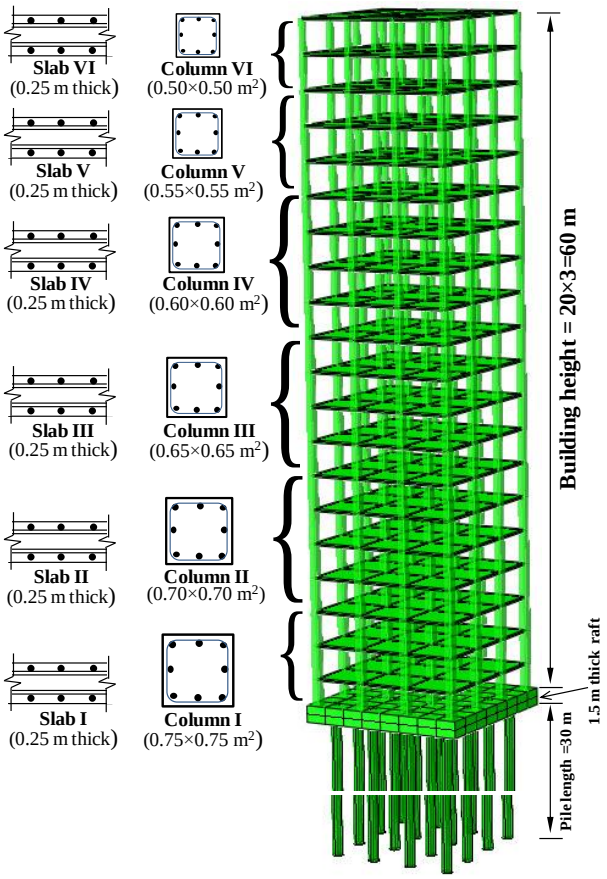

Fig. 2 Designed sections of columns and slabs

allowable foundation settlement of 50 mm given by Skempton and MacDonald (1956) and O' Brien (2012).

2.2 Features of the building

Fig. 2 illustrates the building and its sections of structural components. The structural sections were adopted from Rasouli and Fatahi. 2019. They designed the sections by conducting a routine design procedure by conducting analysis and design using SAP2000 based on AS3600, AS1170.1, and AS1170.4. The details of all sections are summarized in Table 2. The specific compressive strength (f_c') and mass density of the concrete members were considered to be 32 MPa and 2400 kg/m3 respectively, and the modulus of elasticity of concrete was estimated to be equal to 30.1 GPa.

2.3 Characteristics of the numerical model

Fig. 3 shows the finite element mesh developed in Abaqus software for case S. The different structural components of the building (i.e., columns and slabs) were modelled by using 2-node linear beam elements (B31), and four-node shell elements (S4). The mechanical behaviour of structural elements of the building were modelled using an elastic-perfectly plastic constitutive model to capture any possible inelastic behaviour of the structural elements; these structural elements could behave elastically until they reached yielding stress that was equal to the compressive strength of concrete (i.e., f_c'= 32 MPa) taken from study of Shing and Tanabe (2001). The solid element with 8-node brick, trilinear displacement, trilinear pore pressure (C3D8P) was used to model soil. Coupled-consolidation analysis was performed to simulate accumulation of excess pore water pressure. The finite element method has inherent limitations that make it difficult to capture shear localization in the soil since the shear band generally develops in a zone of one element wide (i.e. element size) (Ni *et al*. 2018b, Hu *et al*. 2021). Dudoignon *et al*. (2001) reported the reorientation and crushing of kaolin clay particles occurring in a shear band of thickness 20-30 mm. The dimensions associated with the centrifuge tests (conducted at 100 times the normal gravity) were utilized for the numerical modeling. Numerical difficulties were produced and errors were obtained with element size of 30 mm. The sensitivity of the numerical results with respect to size of mesh was explored and it was found that without undermining stability of analysis, the optimum value 1.5 mm of element width (50 times the shear band thickness) was chosen. A relatively fine mesh was used near the piled raft and tunnel because large shear strains were expected and the mesh became coarser further away from the tunnels.

In previous studies, many researchers used different soil models to investigate tunnelling related problems. Some researchers adopted elasto-plastic model with Mohr-Coulomb failure criterion (Lee 2012a, b, Mroueh and

Table 3 Model parameters of kaolin clay adopted in the parametric study

Description	Parameter	Reference
Effective angle of shearing resistance at critical state: ϕ'	22°	(Powrie 1986)
Parameter controlling the slope of the isotropic normal compression line in the ln(1 + e) versus lnp plane, λ^*	0.11	(Al-Tabbaa 1978)
Parameter controlling the slope of the isotropic normal compression line in the ln(1 + e) versus lnp plane, κ^*	0.026	(Al-Tabbaa 1978)
Parameter controlling the position of the isotropic normal compression line in the ln(1 +e)–lnp plane, N	1.36	(Al-Tabbaa 1978)
Parameter controlling the shear stiffness at medium- to large- strain levels, r	0.65	(Parry and Nadarajah 1974)
Parameter controlling initial shear modulus upon 180° strain path reversal, m_R	14	(Benz 2007)
Parameter controlling initial shear modulus upon 90° strain path reversal, m_T	11	(Benz 2007)
Size of elastic range, R	1×10^{-5}	(Benz 2007)
Parameter controlling the rate of degradation of the stiffness with strain, β_r	0.1	(Benz 2007)
Parameter controlling degradation rate of stiffness with strain, χ	0.7	(Benz 2007)
Initial void ratio, e	1.05	Deduced from measured water content
Dry density (kg/m^3)	1136	Deduced from measured void ratio
Coefficient of permeability, k (m/s)	1×10^{-9}	(Al-Tabbaa 1978)

Shahrour 2003, Xiang *et al.* 2008), the Drucker–Prager model (Lee and Ng 2005, Soomro *et al*. 2015), or the hardening soil model (Lee *et al*. 2012, Mica *et al*. 2009, Yang *et al*. 2011) to predict tunnel-induced ground deformation. Reasonable accuracy was achieved in predicting ground movement due to tunnelling. However, wider settlement trough was predicted (Tang *et al*. 2000) because small-strain stiffness was not incorporated in these models. Since the stress-strain relationship of soils is highly nonlinear even at very small strain and the stiffness of soil depends on the recent stress or strain history of the soil (Atkinson *et al*. 1990, Mašín 2005, Xue *et al*. 2021), an advanced hypoplastic model was used to simulate the behaviour of clay in this study. The hypoplastic model (Herle and Gudehus 1999) (Mašín 2005) is able to capture the unique features of behaviour of clay (i.e., small-strain, path and history dependent stiffness as well as stress-state dependent dilatancy). The model parameters were taken from study by (Soomro *et al.* 2020). They calibrated and validated all the parameters of the hypoplastic clay model against centrifuge test results (which was performed to tunnel–soil–pile interaction problems had been demonstrated through back analysis of a centrifuge test (which was performed to investigate the tunnelling effects on pile) available in literature (Loganathan *et al.* 2000). These parameters are summarized in Table 3.

The tunnel excavation was simulated by deactivating soil elements inside the tunnel and applying non-uniform inward displacements to nodes around the boundary of the tunnel, with a pre-defined 1% volume loss (i.e., difference between original volumes to reduced volume). The face of each tunnel section was fixed by applying zero displacement boundary condition to restrain the inward tunnel face movement similar to that in centrifuge tests. Although tunnel lining was not explicitly simulated in the numerical analysis, the effect of this was implicitly included by controlling an equivalent volume loss. Pattern of the applied non-uniform displacement boundaries was determined according to Cheng *et al*. (2007)'s displacement controlled model (DCM). The DCM was proposed based on deformation mechanisms (in green-field) observed in the field and in centrifuge tests.

2.4 Soil structure interactions and boundary conditions

In the analysis, the piled raft installation effect on in situ stress distribution of soil was not considered and hence the "wished-in-place pile" was modelled. Therefore, the behaviour of the pile may be quite close to a bored pile. The obtained computed results can be conservative with this assumption. While modelling tunnel-pile-soil problem, one of the important aspects of modelling soil structure interaction (SSI) is to establish interaction between pile and surrounding soil. Because relative pile soil movement and separation between raft and soil can occur during advancement of tunnelling. To incorporate the interactions between pile-soil and raft-soil, surface- to-surface contact technique provided in Abaqus software package was used.

In this approach, two surfaces in contact were assigned as the master and slave surface. The penalty approach was used for tangential contact and the normal behaviour is modelled as hard contact with no normal relative displacement between the pile and surrounding soil. The interface was modelled by the Coulomb friction law, in which the interface friction coefficient (μ) and limiting displacement (γ_{lim}) are required as input parameters. A limiting shear displacement of 5 mm was assumed to achieve full mobilization of the interface friction equal to $\mu \times p'$, where p' is the normal effective stress between two contact surfaces, and a typical value 0.35 of μ for a bored pile was used in all analyses (Lee 2012a, Soomro *et al.* 2020). Roller and pin supports were applied to the vertical

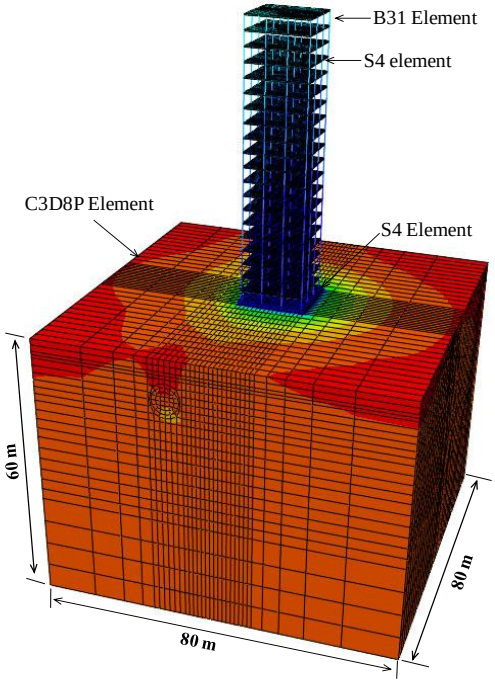

Fig. 3 3D finite element mesh (showing model of building, raft and ground) for case S

sides and the base of the mesh, respectively. Therefore, movements normal to the vertical boundaries and in all directions of the base were restrained. The water table was assumed to be at the ground surface. Initially, the pore water pressure distribution was assumed to be hydrostatic. Free drainage was allowed at the top boundary of the mesh. The tunnel lining was assumed to be continuous and impervious. It is well-known that overconsolidated clays have a preconsolidation pressure higher than the present overburden pressure due to unloading or aging effects. Sivakumar, et al. (2009) stated that the value of coefficient of lateral earth pressure at rest, K_0 is constant during first loading, as an increase in vertical loading also affects the horizontal stress. It implies that K_0 is function of over consolidation ratio (OCR). Hence, the coefficient of lateral earth pressure formula by (Mayne and Kulhawy 1982) (i.e., $K_0 = (1 - sin\varphi')(OCR)^{sin\varphi'}$).

2.5 Numerical simulation

The numerical simulations of all the three cases were carried out in the following steps

(i) Initial geostatic stresses were generated in the mesh by applying gravity load and the coefficient of lateral earth (K_o) value.
(ii) The piles were constructed then raft was placed on top of pile group and soil deposit
(iii) The 20 storey building was constructed on top of the piled raft. A live load of 5 kPa was applied on the floor slab of each storey.
(iv) Excess pore pressure developed in soil mass resulting from dead load of the building and the live load was allowed to fully dissipate.
(v) Three-dimensional tunnel construction was carried out by deactivating soil elements in zone of the tunnel then tunnel lining was installed.

3. Interpretation of computed results

3.1 Settlement of piled raft

Settlement of the piled raft (S_p) induced due to tunnel advancement near pile shaft, next to and below the pile toe in cases of S, T and B, respectively is plotted in Fig. 4. The advancement of tunnel (y) is shown with respect to a monitoring section selected at the mid of pile raft (see inset in the figure). For convenience the S_p and y are normalised by pile diameter (d_p) and tunnel diameter (D), respectively. The numerical predictions in each case show that the induced piled raft settlement increased non-linearly with advancement of tunnel. The piled raft shows signs of the settlement as tunnel reaches at y/D=-5.0. The S_p kept increasing as the tunnel passes through the monitoring section (i.e., at y/D=0) until the tunnels reached at y/D=+5.0. It implies that an influence zone (in which the building is affected by nearby tunnel excavation) can easily be identified. The influence is comprised of distance equal to five times of tunnel diameter ahead and beyond the monitoring section (i.e.-5.0≤ y/D ≤+5.0). Among the three cases, the largest and smallest settlement were predicted when tunnel was excavated near the pile shaft (case S) and below the pile toe (case B), respectively. This was because of the plastic strain generated surrounding the piles due to tunnel-induced stress release (discussed in section 3.6). Since the tunnel is located adjacent to pile shaft in case of S, the shafts of the piles were affected by tunnelling-induced plastic strain. However, the toes of the piles were resting on the intact (from plastic strain) stiffer layer. Whereas, toes of

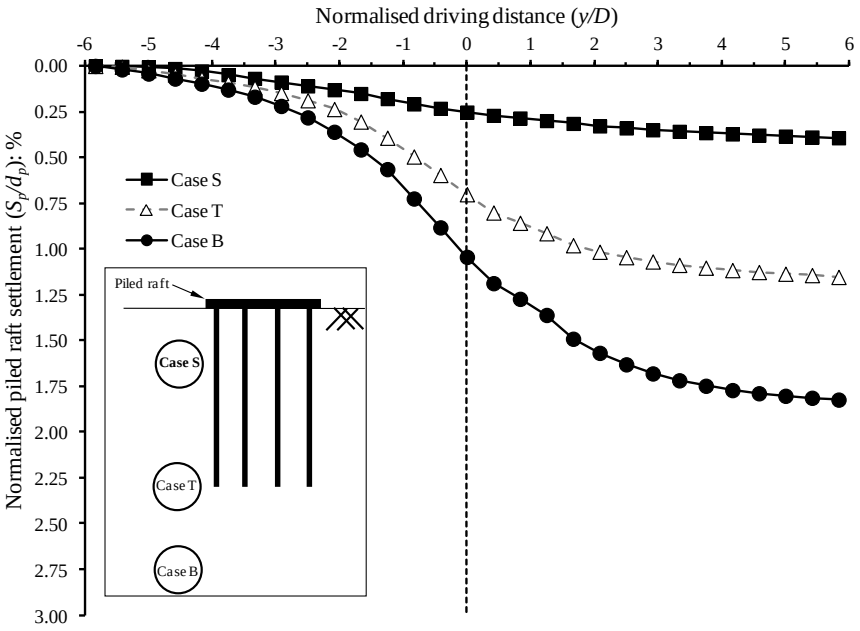

Fig. 4 Piled raft settlement due to advancement of tunnelling

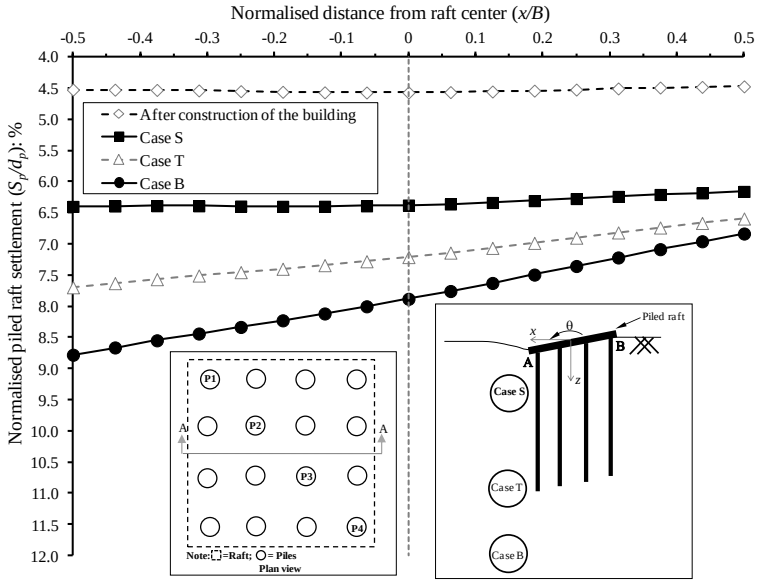

Fig. 5 Evolution of differential settlement in the raft

the piles were severely influenced by the plastic strain due to advancement of tunnelling adjacent to and below the pile toes (in cases of S and T, respectively). Consequently, the piled raft experienced the larger settlement in case of T and B than that in case of S. On the other hand, because of shallow in case of S and deeper tunnel in case of B, the surface settlement is the largest and smallest, respectively. On completion of tunnel excavation in cases of S, T and B, the piled raft settlement was $0.40d_p$%, $1.15d_p$% and $1.82d_p$%, respectively. With settlement due to working load (i.e. $4.52d_p$%), the total settlements of the building $4.92d_p$% in case S and $6.34d_p$% in case B exceed the maximum allowable foundation settlement (i.e., 50 mm) according to Skempton and Macdonald (O'Brien 2012) and (Skempton and MacDonald 1956). Hence, the numerical prediction implies that the serviceability limit state of a building founded on pile can be affected when tunnelling activities are performed near or below the pile toes.

3.2 Differential settlement of piled raft

In addition to the discussion of piled raft settlement in previous section, differential settlement induced in the building is an important parameter to investigate. During the tunnel excavation nearby piled raft foundation, as expected, piles closest to tunnel are subjected to larger ground movement and stress-release than those which are farthest from tunnel. As a result, differential settlement is induced in the piles. Fig. 5 shows settlements of piled raft induced at various positions along the centerline of the raft

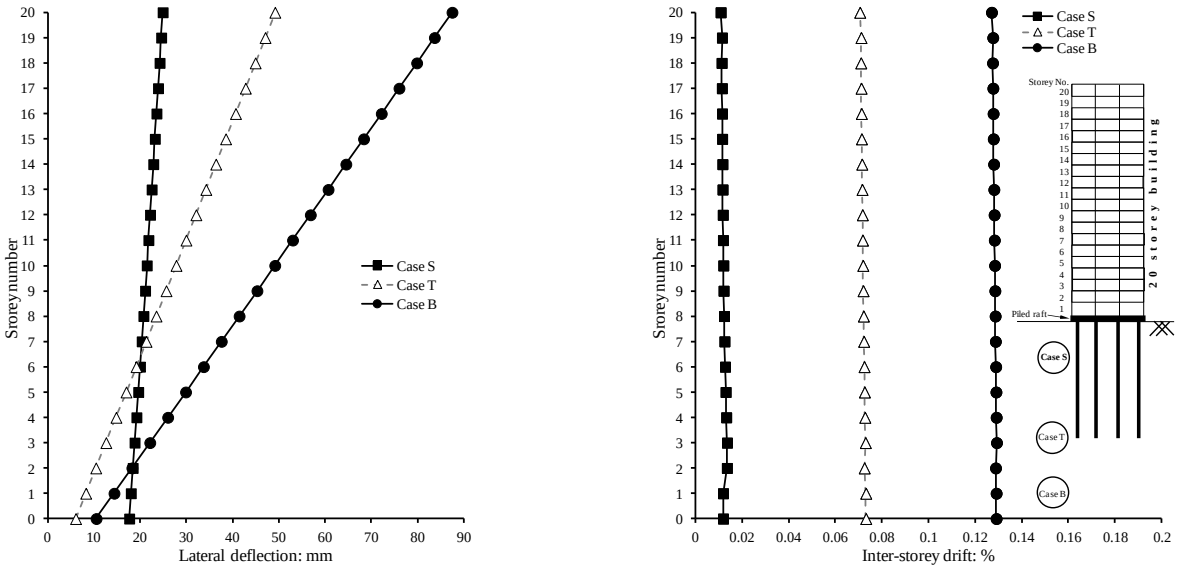

Fig. 6 Lateral deflection and Inter-drift of the building after tunnel excavation

(see inset in the figure) before and after tunnelling in cases of S, T and B. It can be seen that after completion of the building construction (before tunnel excavation), the settlement occurred in the building was uniform through the centerline of the raft. However, as tunnel advanced the raft corner closest to tunnelling settled larger than that of farther from the tunnel. This observation is attributed to tunnelling-induced stress release which is larger and smaller around pile closest to and farthest from the tunnel. The induced differential settlement caused the building permanent inter-storey drifts (discussed in section 3.3.1). As it can be seen from the figure, by increasing the tunnel depth from z_t/L_p = 0.3 in case S to z_t/L_p =1.4 in case B, the differential settlement of the piled raft increased considerably from 2.4 mm to 19.5 mm on completion of tunnel.

3.3 Responses of the building frame

3.3.1 Flooring lateral displacement and inter-storey drifts

The numerical predictions in previous section showed that tunnelling resulted in differential settlement of the raft. This led to displace the 20 storey building laterally towards tunnel in each case. Fig. 6(a) illustrates the induced lateral deflection of the building along each storey on completion of tunnelling in all the three cases (i.e., S, T and B). It can be seen from the figure that lateral deflection increased with height of the building. The maximum lateral deflection occurred at the top of the building (the roof level of 20th storey). The largest and smallest lateral deflection was predicted when tunnel was excavated below the pile toe in case B and near pile shaft in case S, respectively. The general trend of the lateral deflection profile is consistent with differential settlement. Since inter-storey drift may induce distress in structural component of the building, it is necessary to predict the drift induced in the building due to tunnel excavation at different depths.

Fig. 6(b) illustrates inter-storey drift of the building due to tunnel excavation in cases of S, T and B. The inter-storey drift of the building can be defined as ratio of difference of deflections at two storeys to storey height. It is noted that inter-storey drift shows similar trend as that of lateral deflection. Similar to the induced lateral deflection in the building, the inter-storey drift increases with tunnel depth relative to the piles. The induced drift due to tunnel below the pile toe in case B was 11 times larger than that in case S in which tunnel is excavated near the pile shaft. The maximum drift of 0.012%, 0.073% and 0.12% was predicted in cases of S, T and B, respectively.

3.3.2 Induced slope, tilting and distortion in the frame of the building

Tunnelling-induced differential settlement of the raft not only caused building to deflect laterally but also induced slope, tilting and distortion in the frame building. The slope is defined as differential settlement at two points of the frame normalized by horizontal distance between the two settlement points. Moreover, tilting is defined as the ratio of horizontal displacement at the two points to the vertical distance between the two points. Angular distortion is defined as shearing distortion of the frame. Mathematically, angular distortion is calculated as Angular distortion = Slope − Tilting. Fig. 7 shows induced slope, tilt and angular distortion in three bays of the frame (i.e., Bay I, Bay II and Bay III) on completion of tunnelling in cases of S, T and B. The induced slope increased from Bay I to Bay III in each case. As discussed in section 3.2, the differential settlement of piled raft was greater as tunnel was excavated deeper relative to piles. As a result, induced slope as well as tilt was larger in case B as compared to cases S and T. The tilt caused by the building in lateral direction results in lateral movement of the building. Owing to angular distortion induced due to tunnelling in each bay of the

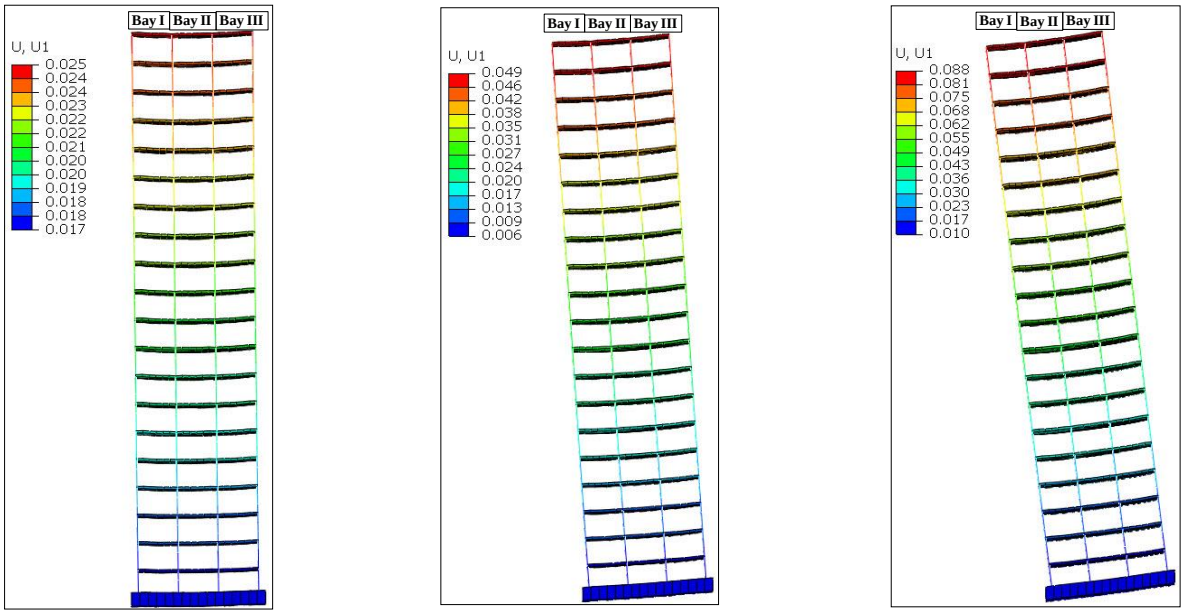

(a) (b) (c)

Multiplying by 10^{-4}	Case S			Case T			Case B		
	Bay I	**Bay II**	**Bay III**	**Bay I**	**Bay II**	**Bay III**	**Bay I**	**Bay II**	**Bay III**
Slope	-0.23	1.60	3.43	6.15	7.50	8.71	11.6	13.1	14.4
Tilt	1.21	1.21	1.21	7.2	7.20	7.2	12.8	12.8	12.8
Distortion	-1.44	0.39	2.22	-1.05	0.30	1.51	-1.3	0.30	1.60
ε_{hs}(T)	-0.013	-0.013	-0.013	-0.012	-0.012	-0.012	-0.012	-0.012	-0.012
ε_{hs}(F)	-0.0018	-0.0042	-0.0035	-0.0028	-0.0032	-0.0019	-0.0031	-0.0031	-0.0016

Fig. 7 Deformation of the building after tunnel excavation in cases of (a) S (b) T and (c) B

frame, each bay underwent an extension at either diagonal line. In case S, the angular distortion and the horizontal strain at top was -1.44×10^{-4} and -0.013×10^{-4} in bay I, and 0.39×10^{-4} and -0.013×10^{-4} in bay II, and 2.22×10^{-4} and -0.013×10^{-4} in bay III, respectively. The angular distortion in each of three bays decreased in cases T and B as compared to case S. The induced angular distortion could incur structural distress in the frame. However, the induced angular distortion in each bay of the building frame in each case is much lower than limiting tolerable value of angular distortion (i.e., 0.002) proposed by (Xiang *et al*. 2008) based on 57 cases of deep foundation.

3.3.3 Horizontal displacement of ground and piled raft and development of shear traction at base of the raft

The computed horizontal displacements at the base of the raft, and in the soils adjacent to the base of the raft developed on completion of tunnel in each case (i.e., S, T and B), are shown in Fig. 8(a). It can be observed from the figure that when tunnel was excavated near pile shaft in case S, significant raft movement in lateral direction was induced compared to lateral movement of the raft in cases of T and B. This is attributed to shear strain generated due to tunnelling around the piles. These observations are opposite to that of differential settlement of the raft. The numerical predictions show that lateral movement of 18 mm, 6 mm and 11 mm was induced in cases of S, T and B, respectively. Compared to horizontal displacement of the ground surface underneath the raft, lateral movement of the raft is substantially higher in magnitude near the edges of the raft. This suggests that clearly sliding occurred at the soil-raft interface. The sliding led in shear traction along the raft (discussed later). However, at the mid-portion of the raft, no relative movement between the raft and adjacent soil was observed in each case.

3.3.4 Development of normal and shear traction at base of the raft

As discussed in previous section that relative soil-raft movement in lateral direction was developed. Consequently, shear traction was generated at base of the raft. The computed normal and shear traction after construction of the building (before tunnelling) and on completion of tunnel

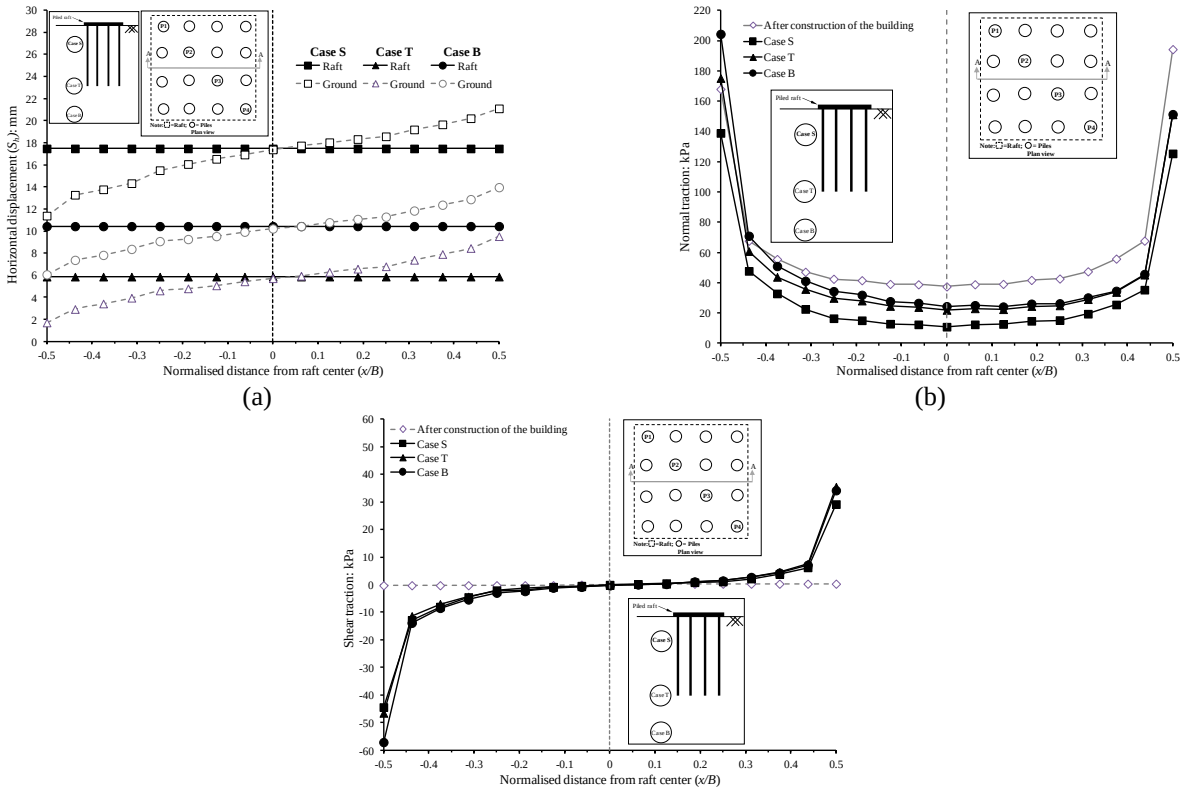

Fig. 8(a) Horizontal displacement of ground and piled raft, (b) Normal traction; and (c) Shear traction on the raft ba se along the cross-section A-A

in each case (i.e., S, T and B) are plotted in Figs. 8(b) and 8(c), respectively. The compressive normal traction and shear traction in positive *x*-direction were taken as positive. It can be seen from Fig. 8(b), construction of tunnel caused normal traction to decrease in each case. This is because load transferred from the raft to the piles (discussed later). Consistent with these redistributed normal tractions, additional settlement developed, which act to reduce the differential settlements induced in the building. It can clearly be seen that shear traction is mobilized over most of the raft portion except mid-portion of the raft (i.e. $-0.125 \leq x/B \leq 0.25$). This is because of large normal traction and less relative raft soil displacement in that portion.

3.4 Changes in load taken by the raft during tunnel excavation

After construction of the building resting on a piled raft system, some of the building load is sustained by the raft and remaining load is transferred to the piles. However, the load taken by the raft can be altered when tunnelling activity is performed close to piles. Fig. 9 represents the change in load sharing by the raft during advancement of twin tunnels in cases S, T and B. It can be seen that before tunnelling (after application of working load), about 7.55%of the building load (i.e. 57.6 MN) was carried by the raft and rest of the load was transferred to sixteen piles. In case of S, the load taken by the raft kept decreasing during the entire process of tunnelling. As the second tunnel approaches the monitoring section, rate of reduction of the load is the highest but as it passes through the monitoring section, no further reduction was predicted. This indicates that the building load was transferred to piles on completion of tunnel. This can be attributed to separation of the raft and the ground because of induced larger ground surface settlement and lesser piled raft settlement. As a result of the gap between the raft and the ground, normal traction decreased (see Fig. 8(b)) on completion of tunnelling. In contrast to case S, the load taken by the raft firstly decreased then increased as tunnel approached the monitoring section in both cases T and B. This implies that the load is transferred to the raft. This is because the tunnelling in both the cases led to substantial settlement in the raft (see Fig. 4) which was less than tunnelling-induced ground surface settlement. The maximum percentage increment of the load carried by the raft on completion of the tunnelling in case of T and B were 3% and 5%, respectively.

3.5 Changes in axial load distribution along piles

As discussed in previous section, the load taken by the raft altered substantially due to tunnel excavation in each case. It suggests that changes in axial load distribution along 16 piles can be induced. Since arrangement of the 16 piles in the piled raft system is in square pattern (i.e., 4×4 piles), the piles at critical positions are selected for discussion in this section. The piles are designated as P1, P2,

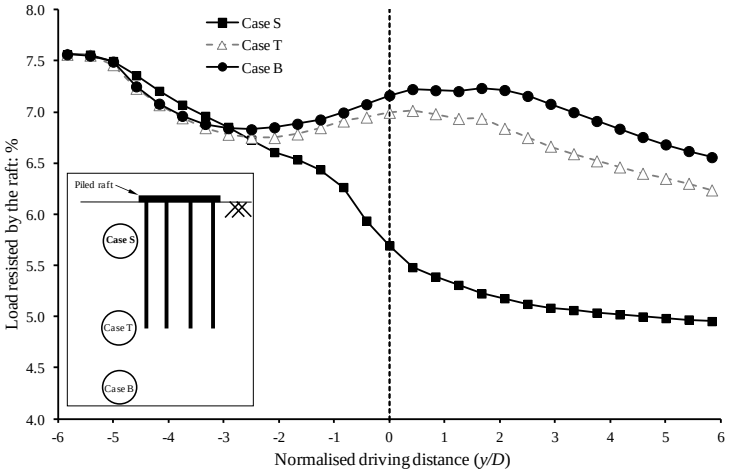

Fig. 9 Changes in load resisted by the raft during tunnel advancement

P3 and P4 (see the inset in Fig. 10). Figs. 10(a)-10(d) compare axial load distribution along the lengths of piles P1, P4, P2 and P3, respectively in cases S, T and B. For comparison, load distribution along the length of each pile before tunnelling is included in each figure. It can be observed from the figure that the load taken by the piles positioned at the corner of the raft (i.e., P1 and P4) is same before tunnelling. Before tunnelling, the load taken by the piles P1 and P4 is 5050 kN. Both piles resisted the load by shaft resistance (77% of the load) and remainder resisted by the piles end-bearing. In case S, the axial load along upper portion of pile P1 ($Z/L_p \leq 0.56$) increased after tunnelling. This indicates that shaft resistance decreased along that portion of pile P1. This observation can be attributed to tunnelling-induced shear stain due to stress release at the mid-portion of the pile (discussed in section 3.6). To support the load, shaft resistance was mobilised at lower portion of the pile (Z/L_p=0.5). Unlike in case S, the axial load distribution along the entire length of pile P1 was reduced in cases T and B. This prediction implies that end-bearing reduced and shaft resistance was mobilised along the entire length of the pile. This is because of location of tunnel in both cases T and B. The tunnelling-induced shear strain is around and below the pile toe in case of T and B, respectively. This led the end-bearing of the pile to reduce and consequently shaft resistance was mobilised to carry the load. On the other hand, negligible changes were found in axial load distribution of pile P4 due to tunnelling in each case (see Fig. 10(b)). This may be because the location of the pile P4 is at far side of the tunnelling. It can be seen from Figs. 10(c) and 10(d) that before tunnelling the load transferred to each of pile P2 and P3 was 1600 kN. The piles resisted the load by mobilising shaft resistance (40% of load) along lower portion of the piles and remainder 60% of the load was resisted by end-bearing. It can be seen from the figure that significant load increased along the upper portion of the pile P2 ($Z/L_p \leq 0.56$) in case S and entire pile length in cases T and B. Similar changes in axial load distribution along the pile length P4 were observed after tunnelling in each case. This load redistribution is ascribed to tunnelling-induced stress release and load transfer from the raft to piles. Further shaft resistance was mobilised along the pile P2 (increased by 27%, 28% and 3% in cases S, T and B, respectively) and pile P3 (increased by 34%. 33% and 11% in cases S, T and B, respectively) to carry the transferred load from the raft.

3.6 Induced deviatoric strain around tunnel and piles

When tunnelling activity is carried out, it inevitably induced stress release in the ground. As a result of stress relief, shear strains are developed around the tunnel. Significant shear strains were developed around the piles when tunnels passed through mentoring section in each case. Figs. 11(a)-11(c) show induced deviatoric strain (in percentage) contours along YOZ plane on completion of tunnelling in cases of S, T and B, respectively.

The green continuous and red dotted contours lines represent compression and extension strains, respectively. For reference, tunnel and piles locations are depicted in the figures. It can be seen from the figure that significant deviatoric strains (around 2% near the tunnel) are developed around tunnel in each case. Since the tunnel location is near pile shaft in case S, the shafts of piles were greatly affected with plastic strains developed due to tunnelling. This suggests that yielding of soil around pile shaft, resulting in reduction of pile shafts (see Fig. 10(a)). On the other hand, the tunnelling-induced plastic strain affected the toe of the piles substantially in cases of T and B. This indicated that the soil yielded at the toe of the piles and below in cases of T and B, respectively. Consequently, the larger settlement of the piled raft was induced in both cases (i.e., T and B) (see Fig. 4). The larger settlement caused the raft to penetrate into the ground led to increase in normal traction (see Fig. 8(b)) which resulted in developed deviatoric strain under the raft.

3.7 Structural response of pile (induced bending moment shear forces along piles)

Before tunnelling, the piles are horizontally confined by the surrounding soil and are subjected to negligible shear forces and bending moments. However, when tunnelling activity is carried near piles and induces stress release in the

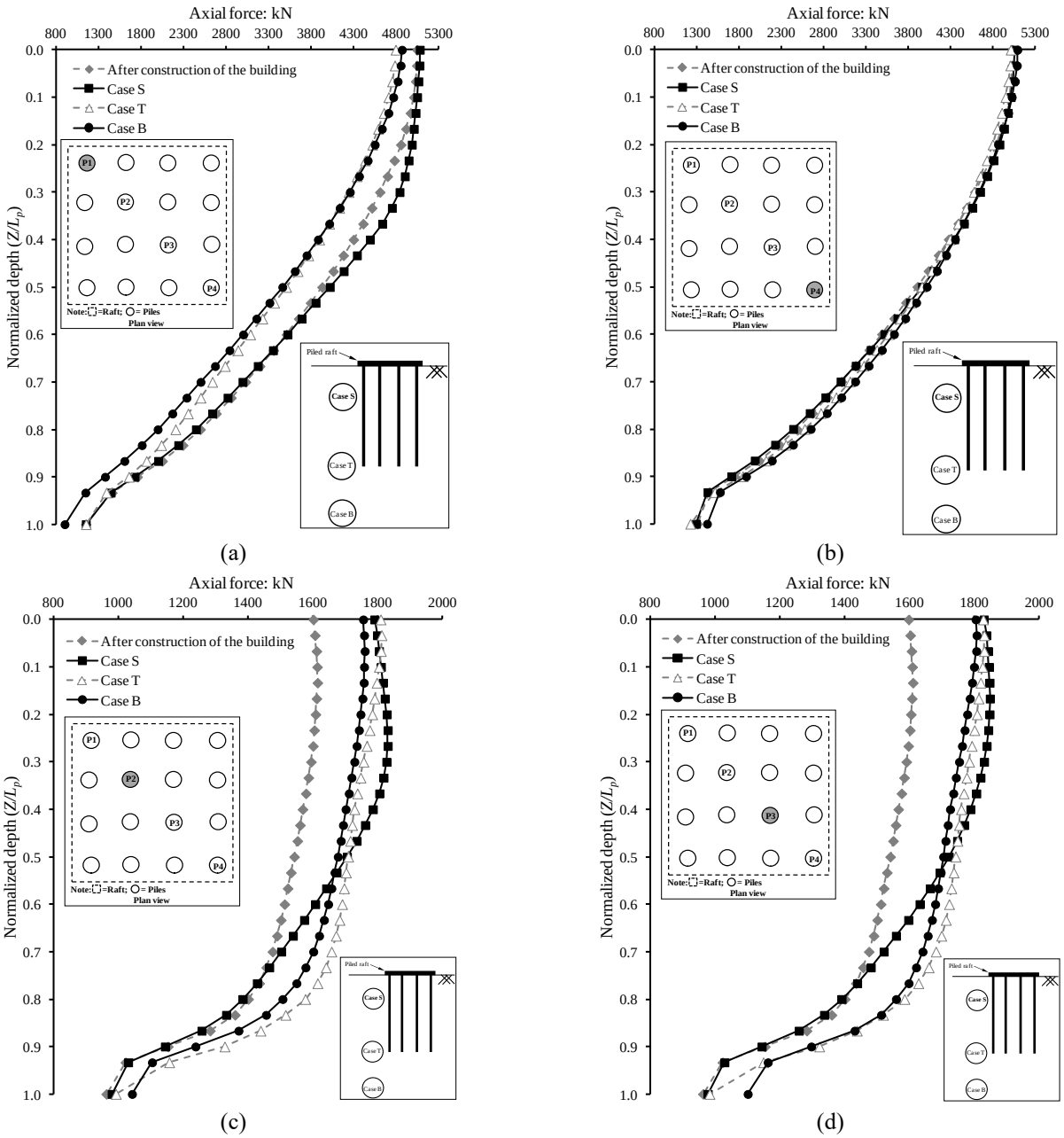

Fig. 10 Axial load distribution before and after tunnelling in each case along

ground, the substantial shear forces and bending moment can be produced in the piles. Thus, the shear forces and bending moment induced along piles due to tunnelling is an important parameter to be predicted. Figs. 12(a)-12(c) illustrate the induced shear forces along normalised depth of four selected piles (i.e., P1, P2, P3 and P4) on completion of tunnel in case of S, T and B, respectively. It is evident from the figures that tunnelling location with respect to piles substantially alters the shear forces distribution in the piles. A highly non-linear shear force distribution was predicted along each pile in each case. Due to rigid connection between the piles and raft, the maximum shear force generated is at head of the piles. In case S, the piles at the corners of the raft (P1 and P4) are subjected to larger shear forces than that placed in the middle of the raft (P2 and P4). The maximum shear forces developed at pile head P1 and P2 were 30 kN and 60 kN, respectively. In addition, shear force with magnitude of 30 kN was induced in pile P1 (closest pile to tunnel). This is because of tunnelling-induced shear strain ground movement towards tunnel (see Fig. 11). Compared to shear forces developed along each pile in case S, the shear forces induced in cases T and B were computed smaller. This is attributed to ground movement due to tunnelling-induced stress release were next to and below pile toe in cases T and B, respectively. Since the piles are mostly designed to carry the vertical load, the bending moment induced in the piles is another important parameter to investigate due to adjacent tunnelling. Figs. 13(a)-13(c) show the induced bending moments along normalised depth of four selected piles (i.e.,

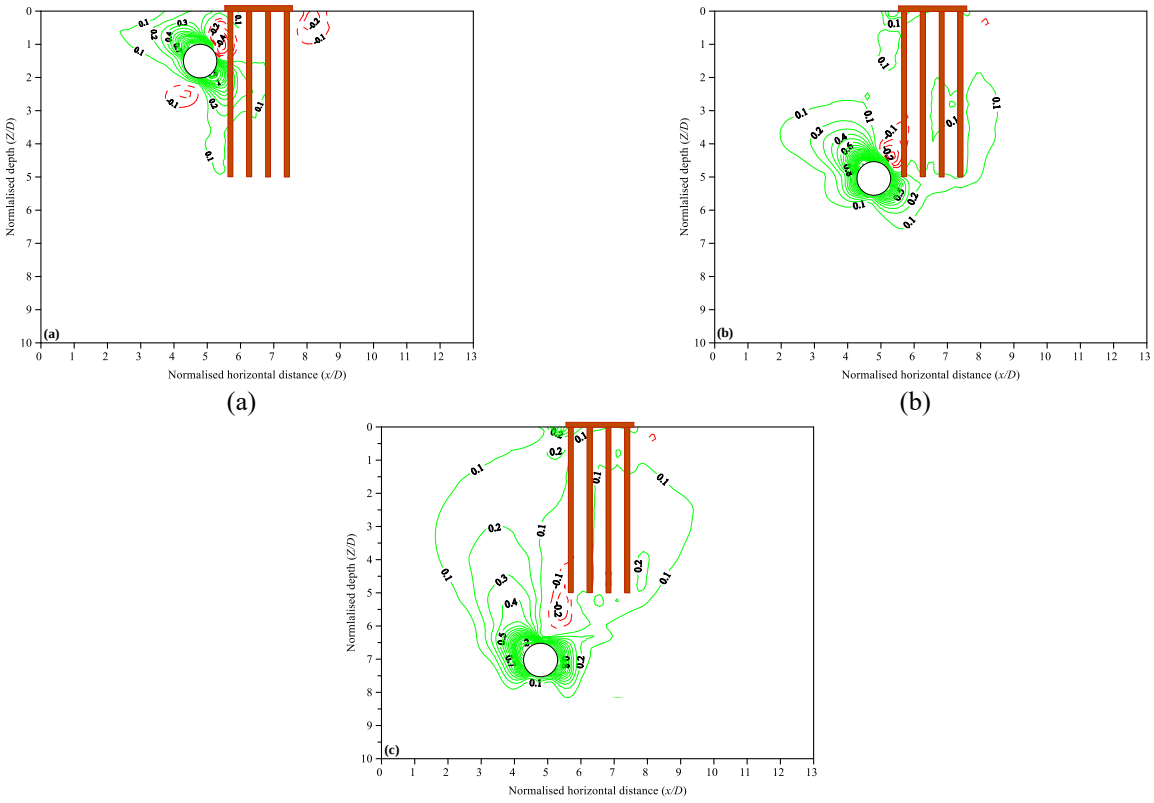

Fig. 11 Induced shear strain in the ground due to tunnelling in cases of (a) S (b) T and (c) B

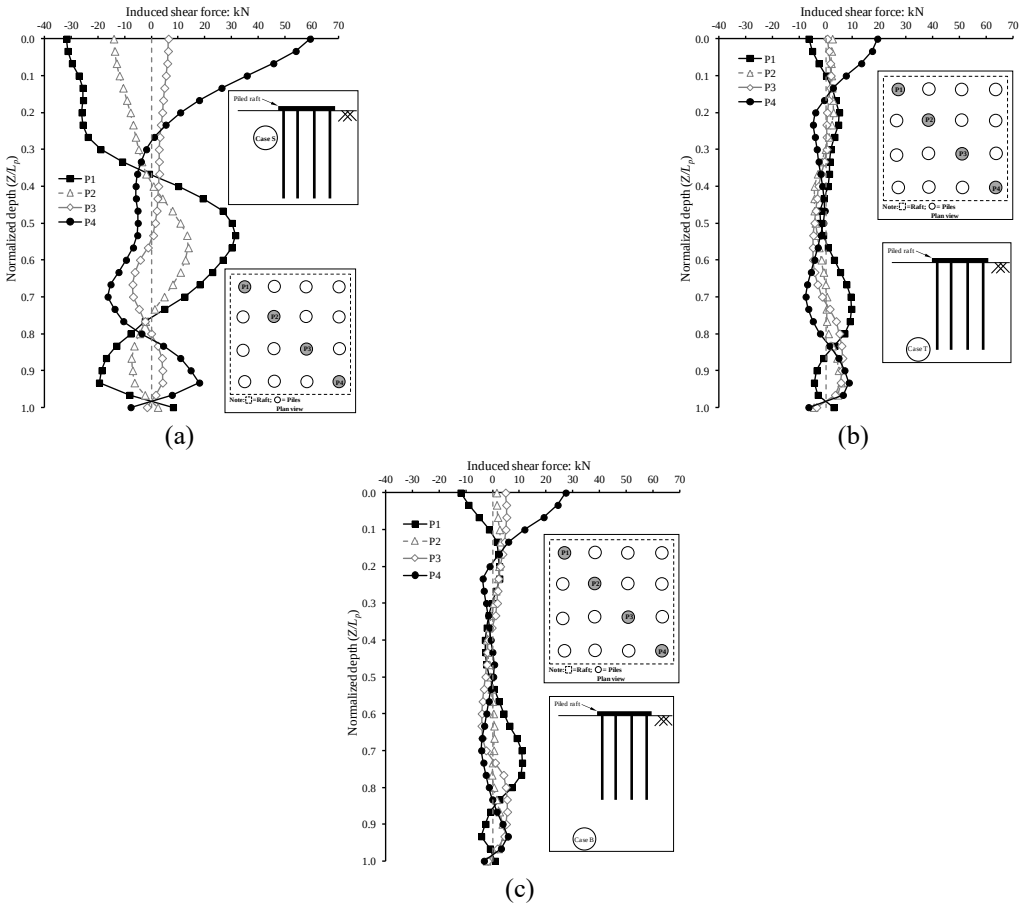

Fig. 12 Induced shear force along four piles (i.e. P1, P2, P3 & P4) in cases of (a) S (b) T and (c) B

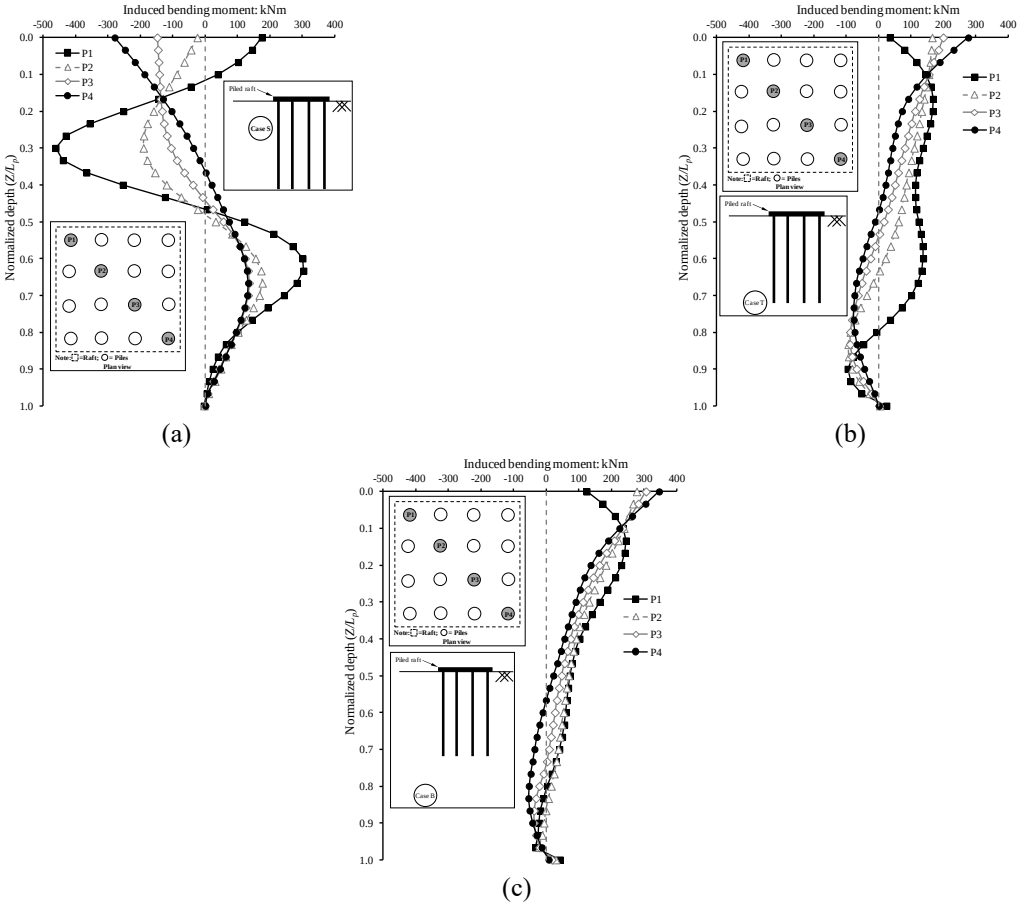

Fig. 13 Induced bending moment along four piles (i.e., P1, P2, P3 & P4) in cases of (a) S (b) T and (c) B

P1, P2, P3 and P4) on completion of tunnel in case of S, T and B, respectively. It is clearly evidence from the figures that the maximum bending moment induced at head of each pile in each case (except pile P1 in case S). This is because the piles are rigidly connected to the raft. In case S, the maximum negative bending moment (460 kNm) was predicted at Z/L_p=0.3 in pile P1. To counter-balance the negative bending moment, moment positive was induced at lower portion of the pile (Z/L_p>0.5). The piles in the middle of the raft (P2 and P3) were subjected to smaller bending moment than that of corner piles due to tunnelling. Since tunnelling activities were performed next to and below pile toe in cases T and B, respectively, the maximum bending moment induced at the head of each pile. The reason can be attributed to induced shear strain in the ground due to tunnelling (see Fig. 11). The magnitudes of the maximum induced bending moments in pile P4 were 275 kNm and 350 kNm in cases T and B, respectively.

4. Conclusions

To understand the deformation mechanism of a 20 storey building sitting on (4×4) piled raft to adjacent 6 m diameter tunnelling in stiff clay, 3D coupled-consolidation numerical modelling was carried out using Abaqus software. The influences of different tunnel locations relative to piles (i.e., z_t/L_p) were investigated in this parametric study. In first case, the tunnel was excavated near the pile shafts with depth of tunnel axis (z_t) of 9 m (i.e., z_t/L_p). In second and third cases, tunnels were driven at z_t of 30 m and 42 m (i.e., z_t/L_p = 1.0 and 1.4), respectively. An advanced hypoplastic clay model (which is capable of taking small-strain stiffness in account) was adopted to capture soil behaviour. This study shows that tunnelling activity adjacent to a building resting on piled raft caused significant settlement, differential settlement, lateral deflection, angular distortion in the building. In addition, substantial bending moment, shear forces and changes in axial load distribution along pile length were induced.

The findings from the parametric study revealed that the building and pile responses significantly Influenced by tunnel location relative to the pile. Based on numerical predictions, the following specific conclusions are drawn:

1. In case B (in which tunnel was excavated below pile toes), the largest settlement, differential settlement, lateral deflection and inter-storey drift was induced as compared to cases S and T (tunnel located near and next to pile toes, respectively).
2. Lateral deflection increased with height of the building. The maximum lateral deflection occurred at the top of the building (the roof level of 20th storey). The largest and smallest lateral deflection was predicted when tunnel was excavated below the pile toe in case B and near pile shaft in case S, respectively.

3. The tunnelling-induced ground movement led to develop shear traction at the raft-soil interface. This is because of lateral movement of the raft is substantially higher as compared to horizontal displacement of the ground surface.
4. In case of S, the load taken by the raft kept decreasing during the entire process of tunnelling.

This indicates that the building load was transferred to piles on completion of tunnel. In contrast, the load taken by the raft is transferred to the raft on completion of tunnelling in both cases T and B.

5. Apart from induced settlement, tilting, angular distortion and lateral movement in the building due to tunnelling, the piles are also subjected to substantial shear forces and bending moment along pile lengths. Compared to shear forces developed along each pile in case S, the predicted shear forces in cases T and B were smaller. In contrast, tunnelling below the pile toes in case B caused the largest bending moment at the head of piles. This is because of rigid connection between raft and pile head and differential settlement due to tunnelling.

It should be noted that the computed results reported in this paper should be treated with caution since they may be specific to the particular soil type, volume loss and modelling techniques adopted.

Acknowledgments

The authors would like to acknowledge the financial support provided by China University of Mining and Technology, Xuzhou, Jiangsu, P. R. China

Conflicts of Interest

The authors declare that they have no conflicts of interest.

References

Al-Tabbaa, A. (1978), "Permeability and Stress-Strain Response of Speswhite Kaolin", PhD thesis, University of Cambridge, UK.

Atkinson, J.H., Richardson, D. and Stallebrass, S.E. (1990), "Effect of recent stress history on the stiffness of overconsolidated soil", *Géotechnique*, **40**(4), 531-540. https://doi.org/10.1680/geot.1990.40.4.531.

Bai, X.D., Cheng, W.C. and Li, G. (2021), "A comparative study of different machine learning algorithms in predicting EPB shield behaviour: A case study at the Xi'an metro, China", *Acta Geotechnica*, **16**(12), 4061-4080. https://doi: 10.1007/s11440-021-01383-7.

Bai, X.D., Cheng, W.C., Ong, D.E. and Li, G. (2021), "Evaluation of geological conditions and clogging of tunneling using machine learning", *Geomech. Eng.*, **25**(1), 59-73. https://doi: 10.12989/gae.2021.25.1.059.

Bai, X.D., Cheng, W.C., Sheil, B.B. and Li, G. (2021), "Pipejacking clogging detection in soft alluvial deposits using machine learning algorithms", *Tunn. Undergr. Sp. Tech.*, **113**, 103908.
https://doi: 10.1016/j.tust.2021.103908

Benz, T. (2007), "Small-strain stiffness and its numerical consequences", *University of Stuttgart, Stuttgart, Germany*,.

Boldini, D., Losacco, N., Bertolin, S. and Amorosi, A. (2018), "Finite element modelling of tunnelling-induced displacements on framed structures.", *Tunn. Undergr. Sp. Tech.*, **80**, 222-231. https://doi.org/10.1016/j.tust.2018.06.019.

Boscardin, M.D. and Cording, E.J. (1989), "Building response to excavation-induced settlement", *J. Geotech. Eng.*, **115**(1), 1-21. https://doi.org/10.1061/(asce)0733-9410(1989)115:1(1)s.

Burd, H.J., Houlsby, G.T., Augarde, C.E. and Liu, G. (2000), "Modelling tunnelling-induced settlement of masonry buildings", *Proceedings of the Institution of Civil Engineers-Geotechnical Engineering*, **143**(1), 17-29. https://doi.org/10.1007/bf02092073.

Burland, J.B., Broms, B.B. and de Mello, V.F.B. (1977), "Behavior of foundations and structures", *Proceedings of the 9th International Conference on Soil Mechanics and Foundation Engineering*.

Caporaletti, P., Burghignoli, A. and Taylor, R. (2005), "Centrifuge study of tunnel movements and their interaction with structures", *Geotechnical aspects of underground construction in soft ground: proceedings of the 5th international symposium TC28, Amsterdam, The Netherlands*. CRC Press, London, UK. https://doi.org/10.1201/noe0415391245.ch10.

Farrell, R.P. (2010), "Tunnelling in Sands and the Response of Buildings".

Franza, A. and DeJong, M.J. (2019), "Elastoplastic solutions to predict tunneling-induced load redistribution and deformation of surface structures", *J. Geotech. Geoenviron. Eng.*, **145**(4), 4019007. https://doi.org/10.1061/(ASCE)GT.1943-5606.0002021.

Franza, A. and Marshall, A.M. (2018), "Centrifuge modeling study of the response of piled structures to tunneling", *J. Geotech. Geoenviron. Eng.*, **144**(2), 4017109. doi:10.1061/(ASCE)GT.1943-5606.0001751.

Franza, A., Marshall, A.M., Haji, T., Abdelatif, A.O., Carbonari, S., and Morici, M. (2017), "A simplified elastic analysis of tunnel-piled structure interaction", *Tunn. Undergr. Sp. Tech.*, **61**, 104–21.

Franzius, J.N., Potts, D.M., Addenbrooke, T.I. and Burland, J.B. (2004), "The influence of building weight on tunnelling-induced ground and building deformation", *Soils Found.*, **44**(1), 25-38. https://doi.org/10.3208/sandf.44.25.

Franzius, J.N., Potts, D.M. and Burland, J.B. (2006), "The response of surface structures to tunnel construction", *Proceedings of the Institution of Civil Engineers-Geotechnical Engineering*, **159**(1), 3-17.

Fu, J., Yang, J., Zhang, X., Klapperich, H. and Abbas, S.M. (2014), "Response of the ground and adjacent buildings due to tunnelling in completely weathered granitic soil.", *Tunn. Undergr. Sp. Tech.*, **43**, 377-388. http://dx.doi.org/10.1016/j.tust.2014.05.022.

Fu, J., Yu, Z., Wang, S. and Yang, J. (2018), "Numerical analysis of framed building response to tunnelling induced ground movements", *Eng. Struct.*, **158**, 43-66. https://doi.org/10.1016/j.engstruct.2017.11.039.

Giardina, G., Van de Graaf, A.V, Hendriks, M.A.N., Rots, J.G., and Marini, A. (2013), "Numerical analysis of a masonry façade subject to tunnelling-induced settlements", *Eng. Struct.*, **54**, 234-247. https://doi.org/10.1016/j.engstruct.2013.03.055.

Goh, K.H. and Mair, R.J. (2011), "Building damage assessment for deep excavations in singapore and the influence of building stiffness", *Geotech. Eng.*, **42**, 1-12. https://doi.org/10.1201/b12748-119.

Herle, I. and Gudehus, G. (1999), "Determination of parameters of a hypoplastic constitutive model from properties of grain assemblies", *Mechanics of Cohesive-frictional Materials: An*

International Journal on Experiments, Modelling and Computation of Materials and Structures, **4**(5), 461-486. https://doi.org/10.1002/(sici)10991484(199909)4:5%3C461::aid-cfm71%3E3.0.co;2-p.

Heama, N., Jongpradist, P., Lueprasert, P., Suwansawat, S. and Jamsawang, P. (2021), "Comparative effects of adjacent loaded pile row on existing tunnel by 2D and 3D simulation models", *Geomech. Eng.*, **27**(2),553-570.

Hu, W., Cheng, W.C., Wen, S. and Rahman, M.M. (2021), "Effects of chemical contamination on microscale structural characteristics of intact loess and resultant macroscale mechanical properties", *CATENA,* **203**, 105361. https://doi: 10.1016/j.catena.2021.105361.

Lee, C.J. (2012a), "Numerical analysis of the interface shear transfer mechanism of a single pile to tunnelling in weathered residual soil", *Comput. Geotech.*, **42**, 193-203. https://doi.org/10.1016/j.compgeo.2012.01.009.

Lee, C.J. (2012b), "Three-dimensional numerical analyses of the response of a single pile and pile groups to tunnelling in weak weathered rock", *Tunn. Undergr. Sp. Tech.*, **32**, 132-142. https://doi.org/10.1016/j.tust.2012.06.005.

Lee, G.T.K. and Ng, C.W.W. (2005), "Effects of advancing open face tunneling on an existing loaded pile", *J. Geotech. Geoenviron. Eng.*, **131**(2), 193-201. https://doi.org/10.1061/(ASCE)1090-0241(2005)131:2(193).

Lee, S.W., Choy, C.K.M., Tse, S.C., Van Gool, F.R., Cheang, W.W. L. and Brinkgreve, R.B.J. (2012), "3D numerical modelling of tunnelling intersecting piles", *Geotechnical aspects of underground construction in soft ground*. CRC Press. https://doi.org/10.1201/b12748-123.

Lee, C.J., Jeon, Y.J., Kim, S.H. and Park, I.J. (2016), "Geomech Eng, 11(4),553-570. https://doi.org/10.12989/gae.2016.11.4.553.

Loganathan, N., Poulos, H.G. and Stewart, D.P. (2000), "Centrifuge model testing of tunnelling-induced ground and pile deformations", *Geotechnique*, **50**(3), 283-294. https://doi.org/10.1680/geot.2000.50.3.283.

Mašín, D. (2005), "A hypoplastic constitutive model for clays", *Int. J. Numer. Anal. Method. Geomech.*, **29**(4), 311-336. https://doi.org/10.1002/nag.416.

Mayne, P.W. and Kulhawy, F.H. (1982), "Ko-ocr relationships in soil", *J. Geotech. Eng.Division*, **108**(6), 851-872. https://doi.org/10.1061/ajgeb6.0001306.

Mica, L., Racansky, V. and Krasny, O. (2009), "Analysis of interaction of retaining walls with underground structures in clay.", *Proceedings of the 2nd Int. Conf. on Computational Methods in Tunneling*.

Mroueh, H. and Shahrour, I. (2003), "A full 3-d finite element analysis of tunneling–adjacent structures interaction", *Comput. Geotech.*, **30**(3), 245-253. https://doi.org/10.1016/s0266-352x(02)00047-2.

O'Brien, A.S. (2012), "Chapter 52 foundation types and conceptual design principles", *ICE manual of geotechnical engineering*. Thomas Telford Ltd.

O'REILLY, M.P. and New, B.M. (1982), *Settlements above Tunnels in the United Kingdom-Their Magnitude and Prediction*. https://doi.org/10.1016/0148-9062(83)91768-0.

Parry, R.H.G. and Nadarajah, V. (1974), "Observations on laboratory prepared, lightly overconsolidated specimens of kaolin", *Geotechnique*, **24**(3), 345-357. https://doi.org/10.1680/geot.1974.24.3.345.

Peck, R.B. (1969), "Deep excavations and tunneling in soft ground", *Proceedings of the 7th ICSMFE*, 1969.

Pickhaver, J.A., Burd, H.J. and Houlsby, G.T. (2010), "An equivalent beam method to model masonry buildings in 3d finite element analysis", *Comput. Struct.*, **88**(19-20), 1049-1063. https://doi.org/10.1016/j.compstruc.2010.05.006.

Potts, D.M. and Addenbrooke, T.I. (1997), "A structure's influence on tunnelling-induced ground movements", *Proceedings of the Institution of Civil Engineers-Geotechnical Engineering*, **125**(2), 109-125. https://doi.org/10.1680/igeng.1997.29233.

Powrie, W. (1986), "The Behavior of Diaphragm Walls in Clay PhD Thesis. University of Cambridge, UK."

Rasouli, H. and Fatahi, B. (2019), "A novel cushioned piled raft foundation to protect buildings subjected to normal fault rupture.", *Comput. Geotech.*, **106**, 228-248. https://doi.org/10.1016/j.compgeo.2018.11.002.

Ritter, S., Giardina, G., Franza, A. and DeJong, M.J. (2020), "Building deformation caused by tunneling: centrifuge modeling", *J. Geotech. Geoenviron. Eng.*, **146**(5), 4020017. https://doi.org/10.1061/(asce)gt.1943-5606.0002223.

Skempton, A.W. and MacDonald, D.H. (1956), "The allowable settlements of buildings.", *Proceedings of the Institution of Civil Engineers*, **5**(6), 727-768. https://doi.org/10.1680/ipeds.1956.12202.

Son, M. and Cording, E.J. (2007), "Evaluation of building stiffness for building response analysis to excavation-induced ground movements", *J. Geotech. Geoenviron. Eng.*, **133**(8), 995-1002. https://doi.org/10.1061/(asce)1090-0241(2007)133:8(995).

Soomro, M.A., Hong, Y., Ng, C.W.W., Lu, H. and Peng, S. (2015), "Load transfer mechanism in pile group due to single tunnel advancement in stiff clay", *Tunn. Undergr. Sp. Tech.*, **45**, 63-72. https://doi.org/10.1016/j.tust.2014.08.001.

Soomro, M.A., Kumar, M., Xiong, H., Mangnejo, D.A. and Mangi, N. (2020), "Investigation of effects of different construction sequences on settlement and load transfer mechanism of single pile due to twin stacked tunnelling", *Tunn. Undergr. Sp. Tech.*, **96**. https://doi.org/10.1016/j.tust.2019.103171.

Soomro, M.A., Mangi, N., Cheng, W.C. and Mangnejo, D.A. (2020), "The effects of multipropped deep excavation-induced ground movements on adjacent high-rise building founded on piled raft in sand", *Adv. Civil Eng.*, 2020. https://doi.org/10.1155/2020/8897507

Soomro, M.A. (2021a), "3D finite element analysis of effects of twin stacked tunnels at different depths and with different construction sequence on a piled raft", *Tunn.Undergr. Sp. Tech.*, 109, 103759.https://doi.org/10.1016/j.tust.2020.103759

Soomro, M.A., Mangnejo, D.A., Saand, A. and Mangi, N. (2021b), "3D numerical analysis of a masonry façade subjected to excavation-induced ground deformation", *Int. J. Geotech. Eng.*, 1-13. https://doi.org/10.1080/19386362.2021.1937853.

Soomro, M.A., Mangi, N., Mangnejo, D.A. and Memon, N.A. (2021c), "3D centrifuge and numerical modelling of lateral responses of a vertical loaded pile group to twin stacked tunnels", *Eur. J. Environ. Civil Eng.*, 1-28. https://doi.org/10.1080/19648189.2021.1907227

Standards Australia (2002), "Structural design actions; Part 1 Permanent, imposed and other actions", AS1170.1, Sydney Australia: Standards Australia;

Standards Australia (2007), "Structural design actions; Part 4: Earthquake actions in Australia.", AS1170.4, Sydney, Australia.

Standards Australia. 2009a. "Concrete structures.", AS3600, Sydney, Australia.

Standards Australia (2009b), "Piling design and installation.", AS2159, Sydney, Australia.

Tang, D.K.W., Lee, K.M. and Ng, C.W.W. (2000), "Stress paths around a 3-d numerically simulated natm tunnel in stiff clay.", *Geotechnical Aspects of Underground Construction in Soft Ground*, 443.

Taylor, R.N. and Grant, R.J. (1998), "Centrifuge modelling of the influence of surface structures on tunnelling induced ground movements.", *Tunnels and Metropolises*, **1**, 261-266.

Taylor, R., Yip, D. and Jardine, F.M. (2001), "Centrifuge modelling on the effect of a structure on tunnelling-induced ground movements", *Response of Buildings to Excavation-*

induced Ground Movements Conference. CIRIA.
Xiang, Y., Jiang, Z. and He, H. (2008), "Assessment and control of metro-construction induced settlement of a pile-supported urban overpass", *Tunn. Undergr. Sp. Tech.*, **23**(3), 300-307. https://doi.org/10.1016/j.tust.2007.06.008.
Xue, Z.F., Cheng, W.C., Wang, L. and Song, G. (2021), "Improvement of the shearing behaviour of loess using recycled straw fiber reinforcement", *KSCE J. Civil Eng.*, 1-17. https://doi: 10.1007/s12205-021-2263-3.
Yang, M., Sun, Q., Li, W. and Ma, K. (2011), "Three-dimensional finite element analysis on effects of tunnel construction on nearby pile foundation.", *J. Central South Univ.*, **18**(3), 909-916. https://doi.org/10.1007/s11771-011-0780-9.
Yiu, W.N., Burd, H.J. and Martin, C.M. (2017), "Finite-element modelling for the assessment of tunnel-induced damage to a masonry building", *Géotechnique*, **67**(9), 780-794. https://doi.org/10.1680/jgeot.sip17.p.249.

CG